Available online at www.sciencedirect.com
SCIENCE DIRECT®
International Journal of Heat and Mass Transfer 49 (2006) 3968–3976
International Journal of HEAT and MASS TRANSFER
www.elsevier.com/locate/ijhmt

Electrochemical reaction with RedOx electrolyte in toroidal conduits in the presence of natural convection

Shizhi Qian [a], Zongyuan Chen [b], Jing Wang [b], Haim H. Bau [b,*]

[a] Department of Mechanical Engineering, University of Nevada – Las Vegas, 4505 Maryland Parkway, Las Vegas, NV 89154-4027, USA
[b] Mechanical Engineering and Applied Mechanics, University of Pennsylvania, 220 South 33rd Street, Philadelphia, PA 19104, USA

Received 30 June 2005; received in revised form 4 April 2006
Available online 30 June 2006

Abstract

Transport processes in an upright, concentric, annular, electrochemical reactor filled with RedOx electrolyte solution are studied experimentally and theoretically. The electrodes form the two vertical surfaces of the reactor. The theoretical calculations consist of the solution of the Navier–Stokes and the Nernst–Planck equations accounting for species' diffusion, migration, convection, and electrochemical reactions on the electrodes' surfaces as a function of the difference in electrodes' potentials and the average concentration of the electrolyte. Since the convection is driven by density gradients, the momentum and mass transport equations are coupled. The current transmitted through the electrolyte is significantly enhanced by natural convection. The current is measured as a function of the difference in the electrodes' potentials. To obtain the reaction rate constants, an inverse problem is solved and the reaction rate constants are determined by minimizing the discrepancy between theoretical predictions and experimental observations. As an example, we study the reversible electrochemical reaction $Fe^{+++} + e^- = Fe^{++}$ on platinum electrodes.

Keywords: Electrochemistry; RedOx; Natural convection; Rate constants estimation; Inverse problem; Computational electrochemistry; Electrochemical reactor

1. Introduction

Electrochemical reactors are of interest for processes ranging from energy conversion to material deposition and production to propulsion. When an electric current is transmitted in an electrochemical reactor, the resulting concentration gradients in species induce density gradients, which, in turn, drive natural convection. Often, the convective motion plays an important role in the transport processes that occur in the reactor. For example, the convective motion may greatly increase the electric flux's magnitude and non-uniformity and may cause non-uniform material deposition during electroplating. Thus, it is not surprising that the study of natural convection in electrochemical reactors has attracted considerable attention [1–15].

A theoretical investigation of the performance of the electrochemical reactor requires one to simultaneously solve the momentum and Nernst–Planck equations with nonlinear boundary conditions describing the electrochemical reactions at the electrodes' surfaces. The solution of these equations is not trivial, and many investigators have made simplifying assumptions such as carrying out the calculations only under limiting current conditions [8,9,12,14] to avoid the need to account for electrode kinetics. In contrast, we solve the full problem using the nonlinear Butler–Volmer expression for the electrochemical reactions on the surfaces of the electrodes and accounting for migration in the electrolyte solution.

Our interest in electrochemical reactors was inspired by our work with magneto-hydrodynamic (MHD) propulsion

* Corresponding author. Tel.: +1 2158988363; fax: +1 2155736334.
E-mail address: bau@seas.upenn.edu (H.H. Bau).

0017-9310/$ - see front matter © 2006 Elsevier Ltd. All rights reserved.
doi:10.1016/j.ijheatmasstransfer.2006.04.024

Nomenclature

c_i	concentration of species i, mol/m^3
D_i	diffusion coefficient of species i, m^2/s
F	Faraday's constant, C/mol
g	gravitational acceleration, m^2/s
H	height of the reactor
J	current density, A/m^2
k_a	forward reaction rate constant, m/s
k_d	backward reaction rate constant, m/s
m_i	mobility of species i, m^2/(V s)
N_i	flux density of species i, mol/(m^2 s)
p	pressure, Pa
r	radial coordinate
R_U	universal gas constant, J/(mol K)
R_I	inner radius of the toroidal reactor, m
R_O	outer radius of the toroidal reactor, m
T	absolute temperature, K
t	time, s
U	imposed potential on electrode, V
u	velocity, m/s
V	electric potential in the solution, V
z_i	charge number of species i
z	vertical coordinate

Greek symbols

α	charge transfer coefficient
ρ	liquid's density, kg/m^3
ρ_0	water's density, kg/m^3
μ	liquid's visocity, kg/(m s)
η	overpotential, V

in electrolyte solutions. We are considering conduits having rectangular cross-sections with electrodes deposited along the opposing walls. When a potential difference is applied across the electrodes in the presence of a magnetic field that is parallel to the electrodes' surfaces, the resulting current interacts with the magnetic field to produce a Lorentz body force that can propel the liquid. Many conduits may be combined to form a network. By judicious control of the electric potential applied to individually controlled pairs of electrodes, one can propel the electrolyte along any desired path without any mechanical pumps, valves, or moving parts [16]. Miniaturized versions of toroidal reactors of the type studied here can serve as thermal cyclers for DNA amplification in which the reagents are circulated among zones maintained at different temperatures [17], stirrers that enhance mixing [18], heat exchangers [19], and chromatographs with adjustable column lengths [20].

When working with MHD reactors, it is convenient to use RedOx species such as $FeCl_2/FeCl_3$ and potassium ferrocyanide ($K_4[Fe(CN)_6]$)/potassium ferricyanide ($K_3[Fe(CN)_6]$) and inert (i.e., platinum) electrodes. These RedOx electrolytes undergo reversible electrochemical reactions at the electrodes' surfaces without bubble formation, electrode corrosion, and depletion of the electrolyte during operation.

Since we were unable to find the reaction rate constants for $FeCl_2/FeCl_3$, we constructed a toroidal reactor consisting of a 1.75 mm wide and 1.2 mm tall rectangular conduit bent into a torus, filled the reactor with the electrolyte solution, measured the electric current as a function of the electrodes' potential difference, and attempted to match the experimental data with theoretical predictions. In spite of the relatively small dimensions of our reactor, natural convection significantly enhanced the electrical current's magnitude. In order to properly solve the inverse problem, it was necessary to account for natural convection effects. This is the motivation for our study. We focus here on studying the convective flow patterns in the absence of magnetic fields.

Our study has a broader applicability than just our particular application. Knowledge of the convective flow patterns in the annular reactor is also useful for designing and understanding electroplating processes. Furthermore, we demonstrate for the first time the feasibility of predicting the reaction rate constants in the presence of significant natural convection.

The manuscript is organized as follows. Section 2 introduces the mathematical model for the ion transport in the presence of convection and fluid motion driven by density gradients. Section 3 describes the solver validation. Section 4 describes the experimental apparatus. Section 5 provides a summary of the experimental results and describes the reaction parameter estimation and the flow and concentration fields.

2. Mathematical model

Consider an annulus with a rectangular cross-section, an inner radius R_I, an outer radius R_O, a height H, and a width $W = R_O - R_I$ (Fig. 1). We use a cylindrical coordinate system: r, θ, and z centered at the torus' center. r, θ, and z are, respectively, the radial, azimuthal, and vertical coordinates. The two electrodes cover the entire surfaces of the opposing walls of the annulus $r = R_I$ and $r = R_O$. The bottom ($z = 0$) and top ($z = H$) of the conduit are insulated. The conduit is filled with dilute RedOx electrolyte solution. The potential difference imposed across the inner and outer electrodes induces electric current flux $\mathbf{J}(\mathrm{A/m^2}) = J_r\hat{\mathbf{e}}_r + J_\theta\hat{\mathbf{e}}_\theta + J_z\hat{\mathbf{e}}_z$ in the electrolyte solution. Hereafter, bold letters denote vectors. $\hat{\mathbf{e}}_r, \hat{\mathbf{e}}_\theta$, and $\hat{\mathbf{e}}_z$ are, respectively, unit vectors in the r-, θ-, and z-directions. J_r, J_θ, and J_z are, respectively, the components of the current flux in the r-, θ-, and z-directions.

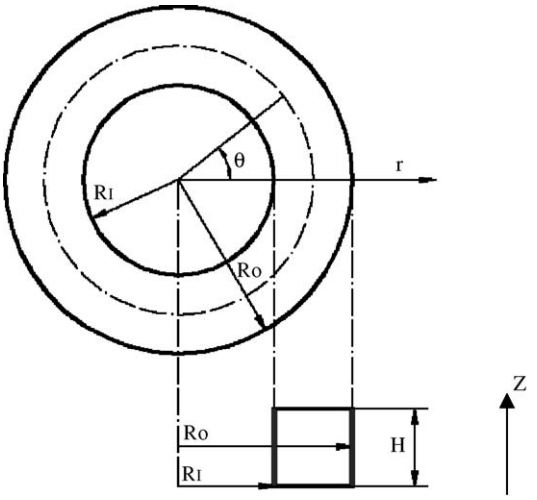

Fig. 1. A schematic of a toroidal conduit with a rectangular cross-section.

The motion of the fluid induced by the electrolyte density variations is described by the continuity and Navier–Stokes equations:

$$\frac{\partial \rho}{\partial t} + \nabla \bullet (\rho \mathbf{u}) = 0 \tag{1}$$

and

$$\rho \frac{\mathrm{D}\mathbf{u}}{\mathrm{D}t} = \rho \mathbf{g} - \nabla p + \mu \nabla^2 \mathbf{u}. \tag{2}$$

In the above, $\mathbf{u} = u_r \hat{\mathbf{e}}_r + u_\theta \hat{\mathbf{e}}_\theta + u_z \hat{\mathbf{e}}_z$ is the fluid's velocity, and u_r, u_θ, and u_z are, respectively, the velocity components in the r-, θ-, and z-directions; t is the time; p is the pressure; $\mathbf{g} = -g\hat{\mathbf{e}}_z$ is the gravitational field; and ρ and μ are, respectively, the liquid's density and viscosity. No-slip boundary conditions are specified at all solid surfaces.

The density of the multi-component electrolyte solution is given by [21]:

$$\rho = \rho_0 + \sum_{i=1}^{N^*} \omega_i (B_{1i} + B_{2i} T^* + B_{3i} \omega_i), \tag{3}$$

where ρ_0 is the density of pure water; B_{ki} are coefficients for the ith electrolyte component (Table 1.2 in [21]); T^* is the temperature in °C; $\omega_i = \frac{M_i [c_i]}{1000\rho}$ is the mass fraction of the ith electrolyte component, and M_i and $[c_i]$ are, respectively, the molecular mass (g/mol) and molar concentration (mol/m^3) of the electrolyte; and N^* is the number of species in the solution. For the RedOx pair $FeCl_3/FeCl_2$, $N^* = 2$; $[c_1]$ and $[c_2]$ are, respectively, the concentrations of $FeCl_3$ and $FeCl_2$; and M_1 and M_2 are, respectively, the molar masses of $FeCl_3$ and $FeCl_2$.

When the RedOx couple $FeCl_3/FeCl_2$ is used, the electrolyte solution contains the cations Fe^{3+} and Fe^{2+} and the anion Cl^-. More generally, the RedOx electrolyte solution contains K dissolved ionic species ($k = 1, \ldots, K$). The flux densities of dissolved species k due to convection, diffusion, and migration are given by

$$\mathbf{N}_k = \mathbf{u} c_k - D_k \nabla c_k - z_k m_k F c_k \nabla V, \quad k = 1, \ldots, K \tag{4}$$

assuming that the electrolyte solution is dilute and the salt completely decomposes into ions. In the above, c_k is the molar concentration, D_k is the diffusion coefficient, z_k is the charge number, and m_k is the mobility of the kth ion species. F is Faraday's constant, and V is the electrical potential in the electrolyte solution. The flow field $\mathbf{u}$ is determined by simultaneously solving the continuity and Navier–Stokes equations (1) and (2). Using the Nernst–Einstein relation, the mobility is expressed in terms of the diffusivity D_k, the universal gas constant R_U, and the absolute temperature T.

$$m_k = \frac{D_k}{R_U T}, \quad k = 1, \ldots, K. \tag{5}$$

The concentration of each species is governed by the Nernst–Planck equation [22,23]:

$$\frac{\partial c_k}{\partial t} + \nabla \bullet \mathbf{N}_k = 0, \quad k = 1, \ldots, K. \tag{6}$$

In the above, we assume that there are no homogeneous reactions.

Eq. (6) consist of $K + 1$ unknown variables: the concentrations of the K dissolved species and the electric potential V. The electroneutrality condition provides the (K+1)th equation:

$$\sum_{k=1}^{K} z_k c_k = 0. \tag{7}$$

Since the width of the conduit is much larger than the thickness of the electrical double layer, we do not include the electrical double layer in our model.

The current flux $\boldsymbol{J}$ in the electrolyte solution due to convection, diffusion, and migration is given by

$$\mathbf{J} = F \sum_{k=1}^{K} z_k \mathbf{N}_k. \tag{8}$$

The electroneutrality condition (7) suggests that the convective flux does not contribute directly to the current flux, but it affects the concentration distributions and, hence, the diffusive and migrative fluxes.

The boundary condition for an inert species (no electrode reactions occur for that species) and for all species at the insulated boundaries is

$$\mathbf{n} \bullet \mathbf{N}_k = 0, \tag{9}$$

where $\mathbf{n}$ is the unit vector normal to the surface.

For the RedOx couple, oxidation and reduction reactions occur, respectively, on the surfaces of the anode and cathode:

$$\mathrm{Ox} + ne^- \Longleftrightarrow \mathrm{Red}. \tag{10}$$

When the RedOx couple is the $FeCl_3/FeCl_2$ electrolyte solution, Ox and Red in the above reaction correspond, respectively, to Fe^{3+} and Fe^{2+}, and $n = 1$. The Butler–Volmer equation describes the kinetics of the electrodes' reactions [22–25]:

$$\mathbf{n} \bullet \mathbf{N}_{\mathrm{Red}} = -\mathbf{n} \bullet \mathbf{N}_{\mathrm{Ox}} = k_{\mathrm{a}} c_{\mathrm{Ox}} \mathrm{e}^{\frac{-\alpha n F}{RT}\eta} - k_{\mathrm{d}} c_{\mathrm{Red}} \mathrm{e}^{\frac{(1-\alpha) n F}{RT}\eta}, \quad (11)$$

where c_{Ox} and c_{Red} are the concentrations of the active ions involved in the electrode's reactions (10) at the edge of the electric double layer; α is the charge transfer coefficient for the cathodic reaction, usually ranging from 0.0 to 1.0; n represents the number of electrons exchanged in the reaction, and $n = 1$ for the RedOx couple $FeCl_3/FeCl_2$; k_{a} and k_{d} are, respectively, the forward and backward reaction rate constants;

$$\eta = U - V; \quad (12)$$

U is the imposed potential on the electrode; and V is the potential of the electrolyte solution at the edge of the electric double layer next to the electrode.

Initially, the torus is filled with a well-mixed $FeCl_3/FeCl_2$ electrolyte solution with equal concentrations of $FeCl_3$ and $FeCl_2$ ($[FeCl_3] = [FeCl_2] = C_0$). Then the opposing electrodes are connected to the terminals of a power supply. In view of the angular symmetry, the problem admits axi-symmetric, two-dimensional solutions in the r-z plane. When the reaction parameters $X = (k_{\mathrm{a}}, k_{\mathrm{d}}, \alpha)$ are known, one can solve the forward problem of the coupled mass and momentum equations to obtain the current as a function of the electrodes' potentials [1–15]. When the reaction kinetics are not known, one needs to estimate X by comparing the model's predictions with the experimental results and searching for X values that minimize the discrepancy between the theoretical predictions and the experiments. This is known as the inverse problem. In this paper, we estimate the reaction rate constants of the reversible reaction $Fe^{+++} + e^- = Fe^{++}$ on platinum electrodes in the presence of significant natural convection. The need for these reaction rate constants arose in our work on magneto-hydrodynamic microfluidic networks.

3. Solver validation

To solve the strongly coupled system (Eqs. (1), (2), (6), and (7)), we used the finite element package FEMLAB[1] (version 3.1). We employed non-uniform elements with a larger number of elements concentrated next to the electrodes' surfaces, where concentration boundary layers are expected to be present. We verified that the numerical solutions are convergent, independent of the size of the elements, and satisfy the various conservation laws including current conservation and ion conservation for each of the species. For example, the relative difference $\frac{|I_{\mathrm{a}} - I_{\mathrm{c}}|}{I_{\mathrm{a}}} < 0.01\%$, where I_{a} and I_{c} are, respectively, the current entering the reactor through the anode and leaving the reactor through the cathode. In the interest of space, we omit details.

Our code's predictions compare favorably with numerical solutions available in the literature for electrochemical reactors with specified flow fields [29] and with analytical solutions for magneto-hydrodynamic flow of RedOx electrolytes in the presence of an abundance of supporting electrolyte in planar conduits [30]. Finally, with appropriate selection of reaction parameters, our code predicts well the experimental results reported below.

[1] FEMLAB is a product of COMSOL AB Inc., Sweden (www.femlab.com).

4. Experimental set-up

The experimental apparatus consisted of a toroidal conduit with a 7.2 mm inner diameter, a 10.7 mm outer diameter, and a 1.2 mm height. The reactor was constructed with two 1.6 mm thick sheets of polycarbonate. The toroidal conduit was milled (Fadal 88 HS, Chatsworth, CA) in one slab, and access conduits were milled in the other slab. Electrodes were formed with 50 μm thick platinum sheets bent into cylindrical shells. The platinum sheets were placed along the inner and outer walls of the conduit to form opposing electrodes. Subsequent to the insertion of the electrodes, the two polycarbonate slabs were thermally bonded at 143 ± 1 °C with a hot press (Carver Inc., IN) to form a hermetically sealed reactor with access ports. Fig. 2 is a photograph of the experimental device. The two electrodes were connected to the terminals of a DC-power supply (Hewlett Packard, HP 6032 A), and the potential and current were monitored with a multimeter (Hewlett Packard, HP 3458A). Both the power supply and multimeter were connected to a computer with a GPIB interface. The power supply was controlled and the experimental data was collected and analyzed with LabVIEW (National Instrument, TX, USA). The cavity was filled with the RedOx couple $FeCl_3/FeCl_2$ at various concentrations. The electrolyte solution was prepared by dissolving a weighted mass of $FeCl_3$ and $FeCl_2$ (Fisher Scientific) in known quantities of DI-water. During the experiments, we changed the electrodes' potentials and measured the current as a function of time until steady state conditions were achieved. All the experiments were carried out at room temperature.

5. Results and discussion

In the first, second, and third parts of this section, we present, respectively, the experimental data, the parameter

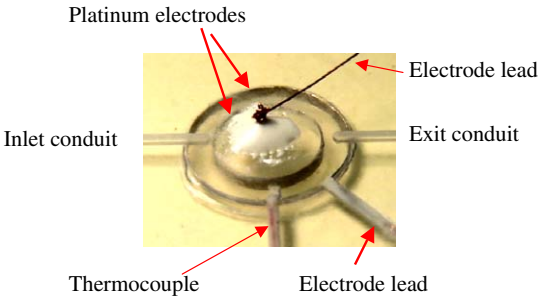

Fig. 2. A photograph of the experimental device.

estimation procedure, and the descriptions of the computed flow and concentration fields.

5.1. Experimental results

Fig. 3 depicts the electric current (mA) as a function of time when the difference in the electrodes' potentials was 1 V at $t = 0$. The electrolyte consisted of equal amounts of ferro and ferri chloride $C_0 = [FeCl_3] = [FeCl_2] = 0.1$, 0.25, 0.4, 0.6, and 0.8 M. The current decayed and after a few oscillations reached a plateau. In all cases, steady current was eventually obtained and maintained indefinitely.

The period of the oscillations, about 400 s, was of the same order of magnitude as the diffusion time constant $(R_O - R_I)^2/D \sim 10^3$ s. As the electrolytes' concentrations increased, so did the amplitude and the duration of the oscillations. When $C_0 \leqslant 0.25$, the fluctuations were barely visible. The magnitudes of the first peaks above the steady state values were approximately 0.04, 0.17, 0.40, and 0.68 mA when $C_0 = 0.4$, 0.6, 0.8 M and 1.0 M, respectively. Roughly, the oscillation's amplitude scaled like $0.75\ C_0^{3.12}$. The oscillatory behavior suggests that natural convection, induced by variations in the density of the electrolyte, played an increasingly important role as the electrolyte concentration increased. The Rayleigh number $Ra = \frac{gH^3|\rho-\rho_0|_{\max}}{\mu D_{Fe^{3+}}} \sim 0.76 \times 10^5$, 1.2×10^5, 1.8×10^5, and 2.8×10^5 when $C_0 = 0.4$, 0.6, 0.8, and 1.0 M. In the above, we adapted the definition for the Rayleigh number suggested by Taylor and Hanratty [31]. In the definition of the Rayleigh number, ρ_0 is the initial density of the electrolyte prior to the transmission of electric current in the solution; ρ is the local density of the electrolyte at steady state obtained by solving the forward problem with the estimated reaction kinetics X (see below); and $|\rho - \rho_0|_{\max}$ denotes the maximum deviation of the electrolyte's density from its average value.

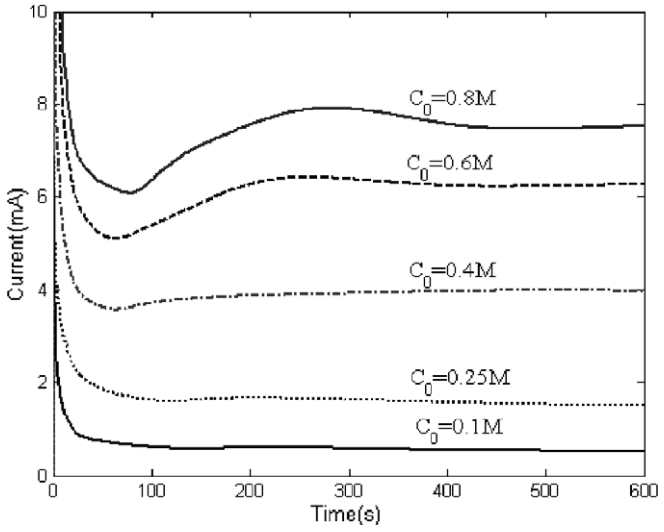

Fig. 3. The current as a function of time when a difference in potentials of 1 V is applied to the electrodes. The average electrolyte concentrations are 0.1 M, 0.25 M, 0.4 M, 0.6 M, and 0.8 M $FeCl_3$ and $FeCl_2$.

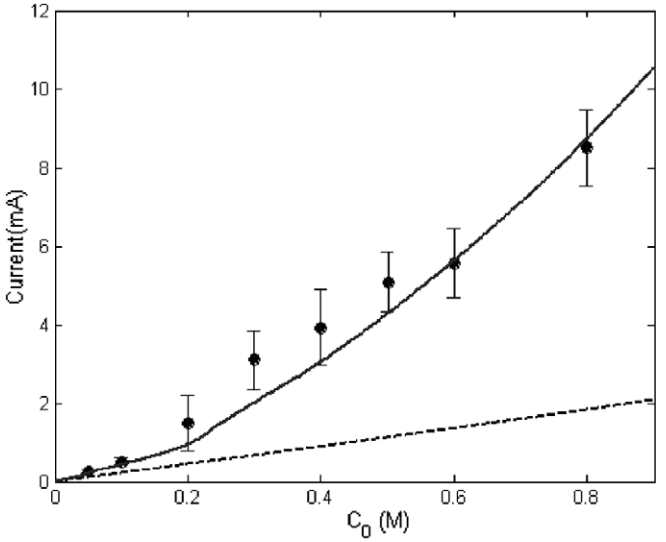

Fig. 4. The steady state current as a function of the electrolyte concentration when the difference in electrodes' potentials is 1 V. The average concentrations $[FeCl_3] = [FeCl_2] = C_0 = 0.1$ M. The solid circles with the error bars, the solid line, and the dashed line represent, respectively, experimental data, theoretical predictions accounting for natural convection effects, and theoretical predictions neglecting natural convection effects.

Fig. 4 depicts the steady state current as a function of the electrolyte's concentration (C_0 in M) when the difference in the electrodes' potentials is 1 V. The solid circles with the error bars correspond to the experimental data. The error bars indicate variations between repeated experiments under seemingly identical conditions. The solid and dashed lines correspond, respectively, to theoretical predictions (to be discussed later) that account for and neglect natural convection effects. As the electrolyte concentration increased, the current increased at a rate of $I \sim C_0^{1.3}$. Since in the absence of natural convection we would expect the current to increase at a rate slower than linear, the superlinear rate of increase provides yet another indication that natural convection plays a significant role in our experiments.

Fig. 5 depicts the steady state current as a function of the difference in the electrodes' potentials when the electrolyte concentration is $C_0 = 0.1$ M. The circles with the error bars correspond to experimental data. The solid and dashed lines correspond, respectively, to theoretical predictions (to be discussed later) accounting for and neglecting natural convection effects. When the difference in the electrodes' potentials was smaller than a certain value (about 0.4 V), the current increased nearly linearly as the difference in electrodes' potentials increased. Once a threshold difference in electrodes' potentials was surpassed, the current saturated at its limiting value.

5.2. Parameter estimation

In this section, we estimate the electrochemical reaction parameters $X = (k_a, k_d, \alpha)$ in the Butler–Volmer equation. To this end, we compute the mean square difference

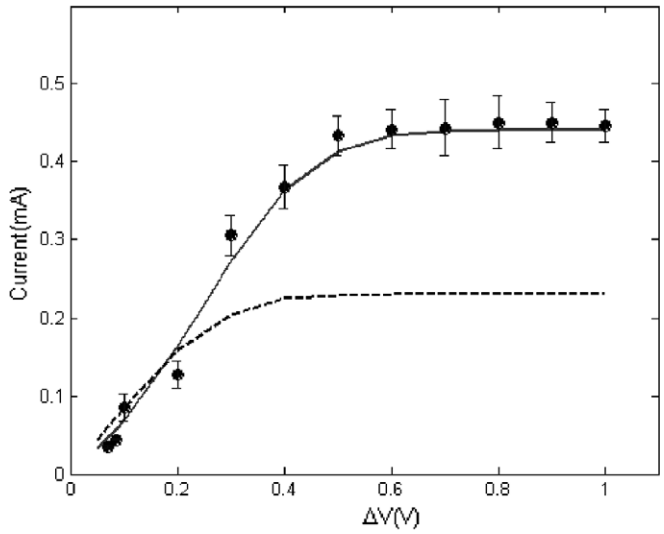

Fig. 5. The steady state current as a function of the difference in electrodes' potentials when the average electrolyte's concentration is 0.1 M $FeCl_3$ and 0.1 M $FeCl_2$. The solid circles with error bars correspond to experimental data. The solid and dashed lines correspond, respectively, to theoretical predictions accounting for and neglecting natural convection effects.

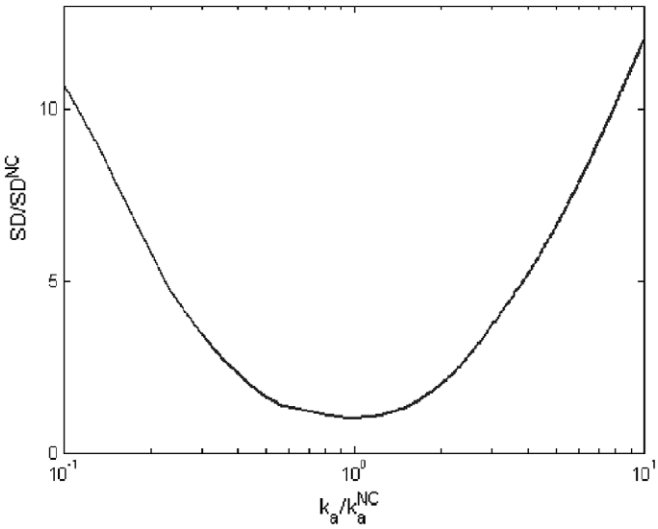

Fig. 6. The normalized mean square error (SD) is depicted as a function of the normalized parameter k_a. Both SD and k_a are normalized with their optimal values.

$$\mathrm{SD} = \frac{1}{KK}\sum_{i=1}^{KK}\left(I_e(i) - I_p(i)\right)^2 \tag{13}$$

between the measured current I_e and the predicted current I_p. The summation is carried out over KK measurements for various differences in electrodes' potentials when the electrolyte concentration is 0.1 M. The objective is to determine the values of $X = (k_a, k_d, \alpha)$ that minimize SD.

We started the optimization process by providing an initial guess for X. We then solved the coupled problem of mass and momentum transfer and computed the electrical currents for various differences in electrodes' potentials when the electrolyte concentration is 0.1 M. In the simulations, we used the diffusion coefficients 6.04×10^{-10}, 7.19×10^{-10}, and 2.032×10^{-9} m^2/s, respectively, for Fe^{3+}, Fe^{2+}, and Cl^- [32]. Steepest descent technique was used to correct the initial guess. The procedure was carried out with Matlab's Optimization Toolbox[2] while the computations of the flow field and current distribution were carried out with the finite element program FEMLAB (version 3.1). The process was repeated until the convergence criteria $|\mathrm{SD}^{(k+1)} - \mathrm{SD}^{(k)}| \leqslant 0.0001$ was satisfied. In the above, $\mathrm{SD}^{(k+1)}$ and $\mathrm{SD}^{(k)}$ were, respectively, the mean square difference at the $(k+1)$ and k iteration steps.

To demonstrate that the process, indeed, converged to the minimum of the function SD, Fig. 6 depicts the normalized error SD as a function of the normalized reaction constant k_a. Both SD and k_a were normalized with their corresponding values at the minimum point. All other parameters except for k_a were maintained fixed. Witness that the curve achieves a minimum at the optimal point. There is no indication of the presence of multiple minima in the optimum's vicinity. Similar figures were drawn (but not shown here) for other parameters.

The calculations were carried out for both a model that neglects and a model that accounts for natural convection. When natural convection effects were accounted for, the estimated optimal parameters were $X^{\mathrm{NC}} = (k_a, k_d, \alpha) \approx (2.2\times10^{-7}\ \mathrm{m/s},\ 7.7\times10^{-8}\ \mathrm{m/s},\ 0.52)$. When natural convection effects were neglected and the process was governed only by diffusion and migration, the estimated parameters were $X^{\mathrm{WC}} = (k_a, k_d, \alpha) \approx (2.8\times10^{-7}\ \mathrm{m/s},\ 1.7\times10^{-7}\ \mathrm{m/s},\ 0.56)$. In the latter case, it was possible to obtain reasonable agreement between the theoretical predictions and the experimental observations only for relatively small differences in potential ($\Delta V \leqslant 0.2$ V).

Using the estimated values listed above, we depicted in Fig. 4 the theoretical predictions for the current as a function of the concentration accounting for (solid line) and neglecting (dashed line) natural convection effects. Not surprisingly, the predictions that neglect natural convection effects grossly underestimated the experimental data. When natural convection effects were accounted for, the theoretical predictions were in good agreement with the experimental observations (symbols).

Fig. 5 depicts the theoretical predictions for the current as a function of the difference in the electrodes' potentials when accounting for (solid line) and neglecting (dashed line) natural convection effects. When natural convection effects are neglected, the theoretical predictions greatly underestimate the experimental data and the predicted limiting current is about 50% of the observed one. When natural convection effects are accounted for, the theoretical predictions are in good agreement with the experimental observations (symbols).

[2] Matlab is a product of MathWorks Inc., USA (www.mathworks.com).

5.3. Description of the flow and concentration fields

To better understand the effects of the induced natural convection on the electrochemical reactions, we simulated the electrochemical reaction with the optimal estimated parameters X^{NC} both neglecting and accounting for natural convection effects.

In the absence of natural convection, Fig. 7 depicts the deviation of the steady state concentrations of the ferric (solid line), ferrous (dashed line) and chloride (dotted line) ions from their average concentrations as functions of the radial coordinate r. A difference in potential of 1 V is applied to the electrodes and the average RedOx electrolytes concentrations are $C_0 = 0.1$ M. When natural convection is absent, the mass transfer process is one-dimensional and the concentrations are independent of the vertical z-coordinate. Contour lines of concentration are simply vertical lines (not shown here). On the surface of the cathode ($r = R_I$), the Fe^{3+} ion is consumed, and the Fe^{2+} ion is produced through reduction. This leads to a lower concentration of the Fe^{3+} ion and a higher concentration of the Fe^{2+} ion next to the cathode. In order to maintain charge neutrality, the concentration of the Cl^- ion is reduced next to the surface of the cathode. On the surface of the anode ($r = R_O$), the ion Fe^{3+} is produced, and the ion Fe^{2+} is consumed through the oxidation reaction, leading to a higher concentration of the ion Fe^{3+} and a lower concentration of the ion Fe^{2+}. The current flux is directed normal to the electrodes' surfaces, and the component in the z-direction is zero in the entire reactor cell. As expected, the product of r and the r-component of the current flux is a constant (i.e., $r \times J_r = \text{constant}$). The concentration of Fe^{3+} next to the cathode ($r = R_I$) equals zero, and the current is at its limiting value.

When natural convection effects are significant, the concentrations of the ions depend on both r and z. Fig. 8 depicts the contours of the ion Fe^{3+}concentration (solid lines) and the streamlines (dash dotted lines) in the reactor under the same conditions as in Fig. 7. The numbers next to the concentration contour lines specify the corresponding concentrations expressed in mol/m^3 or mM. The Rayleigh number $Ra \approx 1675$. The motion consists of two convective cells. Only one cell is shown in the figure. The second cell in the top right corner is very weak and is not depicted. Fe^{3+} ions are advected, respectively, towards and away from the cathode next to the top and bottom of the reactor. The contour lines for the concentrations of ion Fe^{2+} and ion Cl^- are similar to the ones depicted for Fe^{3+}, and, in the interest of space, are not reproduced here. The convective motion enhances the mass transfer between the electrodes and increases the concentration gradients next to the electrodes' surfaces with the net result of increased current through the cell.

The natural convection intensifies as the electrolyte concentration increases. Fig. 9 depicts the concentration contour lines of the ion Fe^{3+} (solid lines) and the streamlines (dash dotted lines) in the reactor cell. The numbers next to the concentration contour lines specify the corresponding concentrations expressed in mol/m^3 or mM. The average bulk concentration of each electrolyte is 0.6 M, and the difference in electrodes' potentials is 1 V. The Rayleigh number $Ra \approx 1.2 \times 10^5$. The motion consists of two counter-rotating convective cells. Both cells are shown in the figure. The concentration contour lines in Fig. 9 are more distorted than in Fig. 8 due to the stronger convection.

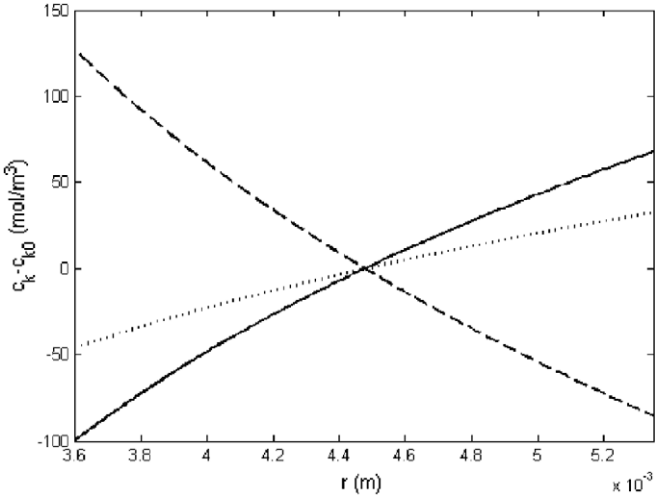

Fig. 7. The steady state deviations of the concentrations of Fe^{3+} (solid line), Fe^{2+} (dashed line) and Cl^- (dotted line) from their average values as functions of r when natural convection effects are neglected. The difference in electrodes' potentials is 1 V and the average concentrations $[FeCl_3] = [FeCl_2] = C_0 = 0.1$ M.

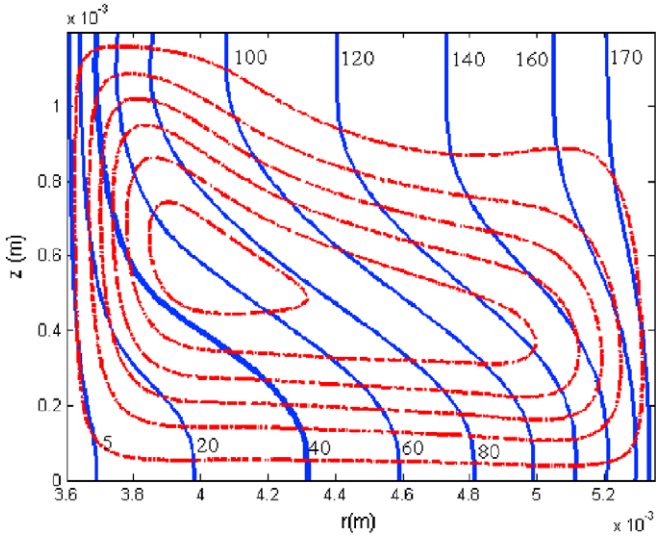

Fig. 8. Contours of the concentration of the ion Fe^{3+} (solid lines) and the streamlines (dash dotted lines) are depicted as functions of r and z. Natural convection effects are accounted for. The difference in electrodes' potentials is 1 V and the average concentrations $[FeCl_3] = [FeCl_2] = C_0 = 0.1$ M. The concentrations labeled in the figure are in mol/m^3.

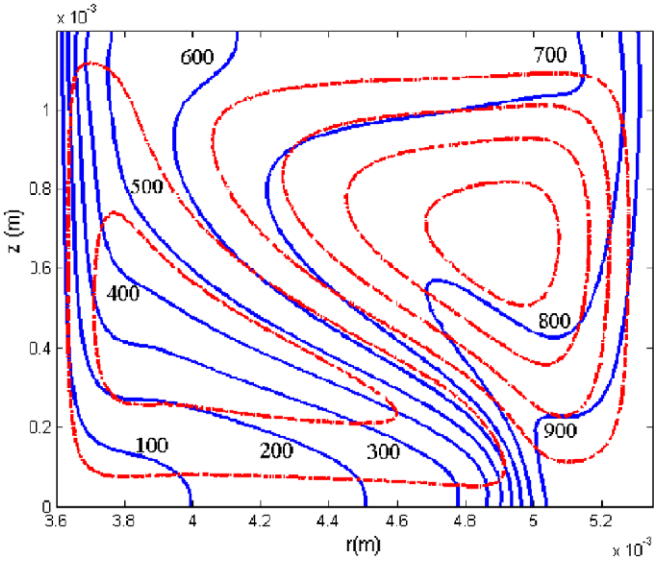

Fig. 9. Contours of the concentration of the ion Fe^{3+} (solid lines) and the streamlines (dash dotted lines) are depicted as functions of r and z. Natural convection effects are accounted for. The difference in electrodes' potentials is 1 V and the average concentrations $[FeCl_3] = [FeCl_2] = C_0 = 0.6$ M. The concentrations labeled in the figure are in mol/m^3.

6. Conclusions

We studied experimentally and theoretically the transport of electric current through an electrolyte solution confined in a toroidal conduit with a rectangular cross-section. The cylindrical shells of the toroid formed opposing electrodes. Experiments and calculations were carried out for electrolyte concentrations ranging from 0.1 M to 0.8 M and difference in electrodes' potentials ranging from 0 to 1 V. The difference in electrodes' potentials was kept below the threshold for water electrolysis. The RedOx electrolyte solution provided a stable operating environment. Once steady-state conditions were established, the current was independent of time. Relatively high currents, without electrode corrosion and bubble formation, were obtained.

The study indicates that natural convection plays a significant role even though the dimensions of the reactor are quite small. Not surprisingly, the natural convection effects increased in importance as the electrolytes' concentration increased. When the difference in electrodes' potentials was below a threshold value, the current increased nearly linearly as the difference increased. Above the threshold value, the current saturated at its limiting value.

Natural convection plays an important role in our experiments. Therefore, when one is estimating the electrochemical reaction parameters, one must account for the natural convection effects. We demonstrated the feasibility of estimating the reaction parameters while fully accounting for convection. The theoretical solutions for the electrical current as a function of the difference in electrodes' potentials and the electrolytes' concentrations were in good agreement with experimental data.

Acknowledgements

The work described in this paper was supported, in part, by a NIH STTR Grant to the University of Pennsylvania (through Vegrandis, LLC) and by the DARPA SIMBIOSYS Program N66001-01-C-8056.

References

[1] P. Carro, S.L. Marchiano, A.H. Creus, S. Gonzalez, R.C. Salvarezza, A.J. Arvia, Growth of 3-dimensional solver fractal electrodeposits under damped free-convection, Phys. Rev. E 48 (1993) R2374–R2377.
[2] D.P. Barkey, D. Watt, Z. Liu, S. Raber, The role of induced convection in branched electrodeposit morphology selection, J. Electrochem. Soc. 141 (1994) 1206–1212.
[3] G. Marshall, P. Mocskos, Growth model for ramified electrochemical deposition in the presence of diffusion, migration, and electroconvection, Phys. Rev. E 55 (1997) 549–563.
[4] G. Marshall, P. Mocskos, H.L. Swinney, J.M. Huth, Buoyancy and electrically driven convection models in thin-layer electrodeposition, Phys. Rev. E 59 (1999) 2157–2167.
[5] G. Marshall, E. Mocskos, F.V. Molina, S. Dengra, Three-dimensional nature of ion transport in thin-layer electrodeposition, Phys. Rev. E 68 (2003) 021607.
[6] M.H. Chung, A numerical method for analysis of tertiary current distribution in unsteady natural convection multi-ion electrodeposition, Electrochim. Acta 45 (2000) 3959–3972.
[7] S. Dengra, G. Marshall, F. Molina, Front tracking in thin-layer electrodeposition, J. Phys. Soc. Japan 69 (2000) 963–971.
[8] A.P. Grigin, A.D. Davydov, Limiting current of electrochemical deposition of copper from copper sulfate and sulfuric acid solution on a vertical electrode under conditions of natural convection, J. Electroanal. Chem. 493 (2000) 15–19.
[9] A.P. Grigin, A.D. Davydov, Limiting current of cathodic copper deposition in solutions containing copper sulfate and nitric acid under conditions of natural convection, Russ. J. Electrochem. 39 (2003) 660–664.
[10] G. Gonzalez, G. Marshall, F.V. Molina, S. Dengra, M. Rosso, Viscosity effects in thin-layer electrodeposition, J. Electrochem. Soc. 148 (2001) C479–C487.
[11] G. Gonzalez, G. Marshall, F. Molina, S. Dengra, Transition from gravito- to electroconvective regimes in thin-layer electrodeposition, Phys. Rev. E 65 (2002) 051607.
[12] D.A. Bograchev, A.D. Davydov, Theoretical study of the effect of electrochemical cell inclination on the limiting diffusion current, Electrochim. Acta 47 (2002) 3277–3285.
[13] D.A. Bograchev, A.D. Davydov, Non-steady-state natural convection in a model electrochemical system with vertical and horizontal plane electrodes, Russ. J. Electrochem. 39 (2003) 967–972.
[14] L.A. Reznikova, E.E. Morgunova, S.A. Lilin, A.D. Davydov, Limiting currents of the triiodide reduction on an inclined disk electrode under conditions of natural convection, Russ. J. Electrochem. 39 (2003) 727–730.
[15] V.M. Volgin, O.V. Volgina, D.A. Bograchev, A.D. Davydov, Simulation of ion transfer under conditions of natural convection by the finite difference method, J. Electroanal. Chem. 546 (2003) 15–22.
[16] H.H. Bau, J. Zhu, S. Qian, Y. Xiang, A magneto-hydrodynamically controlled fluidic network, Sensor. Actuator. B 88 (2003) 207–218.
[17] J. West, B. Karamata, B. Lillis, J.P. Gleeson, J. Alderman, J.K. Collins, W. Lane, A. Mathewson, H. Berney, Application of magnetohydrodynamic actuation to continuous flow chemistry, Lab on a Chip 2 (2002) 224–230.
[18] J. West, J.P. Gleeson, J. Alderman, J.K. Collins, H. Berney, Structuring laminar flows using annular magnetohydrodynamic actuation, Sensor. Actuator. B: Chem. 96 (2003) 190–199.

[19] P.-J. Wang, C.-Y. Chang, Analysis and verifications for meso-scale heat exchanger with magneto-hydrodynamic (MHD) pumps, in: 2003 ASME International Mechanical Engineering Congress, Washington DC, United States, November 15–21, 2003, pp. 359–367.
[20] J.C.T. Eijkel, A. Van den Berg, A. Manz, Cyclic electrophoretic and chromatographic separation methods, Electrophoresis 25 (2004) 243–252.
[21] G.G. Aseyev, Electrolytes Transport Phenomena: Methods for Calculation of Multicomponent Solutions and Experimental Data on Viscosities and Diffusion Coefficients, Begell House, Inc., 1998.
[22] J. Newman, Electrochemical Systems, second ed., Prentice-Hall, Englewood Cliffs, NJ, 1991.
[23] A.J. Bard, L.R. Faulkner, Electrochemical Methods, John Wiley & Sons, New York, 2001.
[24] D.C. Prieve, Changes in zeta potential caused by a dc electric current for thin double layers, Colloids and Surfaces A: Physicochem. Eng. Aspects 250 (2004) 67–77.
[25] M.Z. Bazant, K.T. Chu, B.J. Bayly, Current–voltage relations for electrochemical thin films, SIAM J. Appl. Math. 65 (2005) 1463–1484.
[29] M. Georgiadou, Modeling current density distribution in electrochemical systems, Electrochim. Acta 48 (2003) 4089–4095.
[30] S. Qian, H.H. Bau, Magnetohydrodynamic flow of RedOx electrolyte, Phys. Fluids 17 (6) (2005) 067105.
[31] J.L. Taylor, T.J. Hanratty, Influence of natural convection on mass transfer rates for the electrolysis of ferricyanide ions, Electrochim. Acta 19 (1974) 529–533.
[32] M. Yizhak, Ion Properties, Marcel Dekker Inc., NY, 1997.